EJN European Journal of Neuroscience

FENS Federation of European Neuroscience Societies

European Journal of Neuroscience, pp. 1–11, 2016 doi:10.1111/ejn.13143

Retinal lesions induce fast intrinsic cortical plasticity in adult mouse visual system

Katrien Smolders,[1] Samme Vreysen,[1] Marie-Eve Laramée,[1] Annemie Cuyvers,[1] Tjing-Tjing Hu,[1] Leen Van Brussel,[1] Ulf T. Eysel,[2] Julie Nys[1] and Lutgarde Arckens[1]

[1]Laboratory of Neuroplasticity and Neuroproteomics, Department of Biology, KU Leuven, Naamsestraat 59, B-3000 Leuven, Belgium

[2]Department of Neurophysiology, Medical School, Bochum, Germany

Keywords: immediate early gene, molecular activity, superior colliculus, visual cortex plasticity

Edited by John Foxe

Received 6 May 2015, accepted 1 December 2015

Abstract

Neuronal activity plays an important role in the development and structural–functional maintenance of the brain as well as in its life-long plastic response to changes in sensory stimulation. We characterized the impact of unilateral 15° laser lesions in the temporal lower visual field of the retina, on visually driven neuronal activity in the afferent visual pathway of adult mice using *in situ* hybridization for the activity reporter gene *zif268*. In the first days post-lesion, we detected a discrete zone of reduced *zif268* expression in the contralateral hemisphere, spanning the border between the monocular segment of the primary visual cortex (V1) with extrastriate visual area V2M. We could not detect a clear lesion projection zone (LPZ) in areas lateral to V1 whereas medial to V2M, agranular and granular retrosplenial cortex showed decreased *zif268* levels over their full extent. All affected areas displayed a return to normal *zif268* levels, and this was faster in higher order visual areas than in V1. The lesion did, however, induce a permanent LPZ in the retinorecipient layers of the superior colliculus. We identified a retinotopy-based intrinsic capacity of adult mouse visual cortex to recover from restricted vision loss, with recovery speed reflecting the areal cortical magnification factor. Our observations predict incomplete visual field representations for areas lateral to V1 vs. lack of retinotopic organization for areas medial to V2M. The validation of this mouse model paves the way for future interrogations of cortical region- and cell-type-specific contributions to functional recovery, up to microcircuit level.

Introduction

In mammals, accurately organized cortical retinotopic maps retain the ability to adapt to changes in sensory input well into adulthood (Wiesel & Hubel, 1963; Merzenich *et al.*, 1983; Kaas, 1991; Buonomano & Merzenich, 1998). In cats and monkeys, depriving a small area of primary visual cortex (V1) from its retinal input can cause a dramatic reorganization of its topography. Immediately after inducing small retinal lesions, neurons in the cortical lesion projection zone (LPZ) become inactive, whereas neurons at the border of the LPZ remain responsive but display enlarged receptive fields that are slightly shifted towards the intact retina surrounding the scotoma. Upon longer recovery periods, much larger receptive field shifts take place, which can result in the complete filling-in of the LPZ, at least if the retinal lesions do not exceed 5° in the visual field (Kaas *et al.*, 1990; Heinen & Skavenski, 1991; Chino *et al.*, 1992, 1995; Gilbert & Wiesel, 1992; Chino, 1995; Das & Gilbert, 1995a,b; Dreher *et al.*, 2001; Giannikopoulos & Eysel, 2006; Hu *et al.*, 2009). This spatiotemporal pattern of recovery of neuronal activity from the LPZ border inwards, as measured by electrophysiology, correlates with visual experience-induced changes in expression levels of the activity reporter gene *zif268* in cat V1 (Arckens *et al.*, 2000a,b; Hu *et al.*, 2009). The functional reorganization is believed to involve dynamic structural rearrangements of long-range excitatory horizontal connections as well as compensating modifications of axonal arbors of inhibitory neurons (Yamahachi *et al.*, 2009; Marik *et al.*, 2014).

Despite numerous investigations, hardly any information is available on the impact of retinal lesions outside V1, and unravelling the molecular and cell-type-specific mechanisms underlying the cortical capacity to reorganize neuronal connectivity and functionality calls for the validation of a mouse model (Young *et al.*, 2002; Sawtell *et al.*, 2003; Pham *et al.*, 2004; Tagawa *et al.*, 2005; Hofer *et al.*, 2006a,b; Wandell & Smirnakis, 2009; Huberman & Niell, 2011). Using intrinsic signal imaging strategies, Keck *et al.* (2008, 2011) were able to show that also in the adult mouse a monocular retinal lesion induces a rapid functional recovery, at least in the supragranular layers of contralateral V1. The observed structural adaptations included a very early decrease in the number of spines and boutons on inhibitory neurons in the upper cortical layers, preceding an

Correspondence: Dr L. Arckens, as above.
E-mail: Lut.Arckens@bio.kuleuven.be

increased spine turnover on the apical dendrites of layer V pyramidal cells, followed by the formation of new persistent spines in the later phase of recovery.

To address whether LPZs are induced in- and outside V1 in adult mice by a unilateral retinal lesion we here screened for changes in visually induced *zif268* gene expression throughout the complete visual cortex contralateral to the lesioned eye. This approach facilitated the assessment of a potential region- and layer-specific cortical recovery as well as its timing. To confirm the cortical origin, we also investigated the possible variation in retinal lesion size and the effect of the lesion on the superficial layers of the superior colliculus, the main target of retinofugal axons in mice.

Materials and methods

Animals

Adult C57Bl/6J mice of either sex (n = 26) were housed under standard laboratory conditions with a daily photoperiod of 13 h light and 11 h darkness with water and food available *ad libitum*. All experiments were approved by the ethical research committee of KU Leuven and were in strict accordance with the European Communities Council Directive of 22 September 2010 (2010/63/EU) and with the Belgian legislation (KB of 29 May 2013). Every possible effort was made to minimize the numbers of animals used.

Retinal lesions

Adult mice (n = 23) were sedated by intraperitoneal injection of a mixture of ketamine hydrochloride (75 mg/kg; Dechra Veterinary Products, Eurovet, Heusden-Zolder, Belgium) and medetomidine hydrochloride (1 mg/kg; Orion Corporation, Elanco Animal Health, Brussels, Belgium), and right retinae were focally photo-coagulated (Fig. 1A) with a single IR laser lesion (600 mW, 150–200 ms; 810-nm IR laser, Oculight SLx, Iris Medical, USA) through a laser-adapted operating microscope (Carl Zeiss, Oberkochen, Germany) and focused to the retina with an attached binocular indirect ophthalmo-microscope (BIOM) especially designed for mice using a 132 D lens (SuperPupil XL, Volk, Mentor, OH, USA). The animals were positioned with the right eye facing the BIOM. Due to anaesthesia there were no disturbing head or eye movements. The fundus was observed through the microscope with a 50° field of view. The papilla served as landmark and all lesions were made with the same spot size setting and in the same dorso-nasal position above the optic disc under continuous visual control. The resulting lesions had diameters of about 15° (Fig. 1A). After injection with atipamezol hydrochloride (1 mg/kg; Orion Corporation, Elanco Animal Health) to reverse anaesthesia, the animals were allowed to recover on a heating pad. They were all administered Meloxicam (1 mg/kg; Boehringer Ingelheim Vetmedica, Ingelheim/Rein, Germany) intraperitoneally every 24 h over the next few days as a systematic analgesic. Subsequently, the mice returned to their home cages for different survival times [RL; 2 days (n = 4), 1 week (n = 5), 3 weeks (n = 5), 4 weeks (n = 5) and 8 weeks (n = 4)] before being killed. Adult control mice (CM, n = 3) were maintained in a similar housing and light environment.

Tissue preparation

Prior to being killed, all mice underwent an overnight dark-exposure followed by 45 min of bright light (always between 09.00 and 11.00 h to minimize any possible variation due to time of the day) to obtain an optimal visually evoked immediate early gene (IEG) expression in the cortex (Worley *et al.*, 1991; Zhang *et al.*, 1994; Kaczmarek & Chaudhuri, 1997; Arckens *et al.*, 2000b; Zangenehpour & Chaudhuri, 2002; Van Der Gucht *et al.*, 2007).

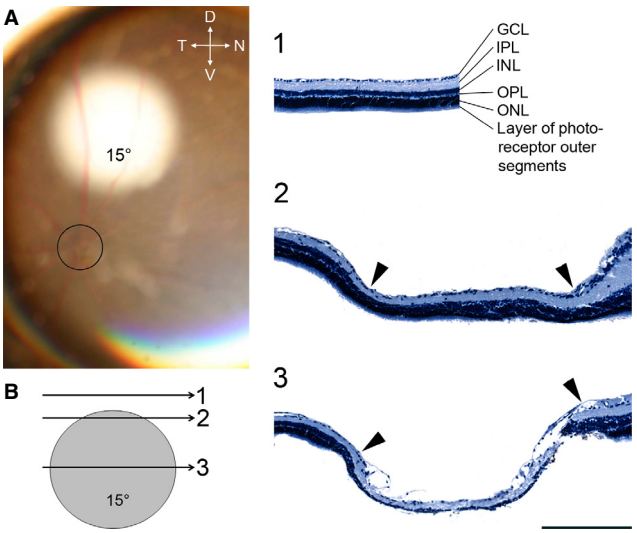

FIG. 1. A permanent retinal lesion. (A) Fundus photograph showing the extent of the 15° retinal lesion in the dorsal part of the nasal retina surrounded by a rim of acute retinal oedema. The black circle indicates the blind spot or optic disc where the optic nerve leaves the eye. (B) Haematoxylin stainings of a retina 8 weeks post-lesion. Panel numbers 1–3 illustrate different positions within the lesion area as depicted in the scheme on the left, with 1 corresponding to a location adjacent to the lesion, 2 being the border of the lesion and 3 a section near the centre of the lesion. Arrowheads indicate the border of the retinal lesion. D, dorsal; N, nasal; T, temporal; V, ventral; GCL, ganglion cell layer; IPL, inner plexiform layer; INL, inner nuclear layer; OPL, outer plexiform layer; ONL, outer nuclear layer. Scale bar: 200 μm.

Animals were killed by cervical dislocation upon deep anaesthesia by an overdose of sodium pentobarbital (600 mg/kg; Ceva Santa Animale, Kansas City, KS, USA) injected intraperitoneally. Brains were rapidly removed and immediately frozen in dry-ice-cooled 2-methylbutane (Merck, Overijse, Belgium) at −40 °C and stored at −80 °C until sectioning. Sections 25 μm thick were prepared on a cryostat (Microm HM 500 OM, Walldorf, Germany), mounted on 0.1% poly-L-lysine (Sigma-Aldrich, St Louis, MO, USA)-coated slides, and kept at −20 °C until hybridization.

Retina histology

To verify retinal lesion size, retinae were stained with haematoxylin following standard procedures. Briefly, eyes were removed from the orbits and hemisected near the ora serrata. After removing lens and vitreous, each eyecup was fixed for 30 min in 4% paraformaldehyde (Sigma-Aldrich) in 0.15 M phosphate-buffered saline (PBS, pH 7.42) and embedded in paraffin (McCormick Scientific, St Louis, MO, USA). Sections 7 μm thick were cut on a microtome (Microm HM 360), collected on Mayer's albumin (Prosan, Merelbeke, Belgium)-coated Superfrost Plus slides (Menzel-Gläser, Braunschweig, Germany), stained for 15 min in a haematoxylin solution (0.1% haematoxylin, 0.02% sodium iodate, 5% potassium aluminum sulphate, 0.1% citric acid) and coverslipped.

The variation of the extent of the retinal lesion (n = 5) was calculated by multiplying the number of sections on which the lesion was visible by their thickness, taking the intersection interval into account.

In situ hybridization

In situ hybridization was performed as previously described (Arckens *et al.*, 1995; Nys *et al.*, 2015). Series of coronal brain sections between Bregma levels −2.70 and −4.84 were analysed to examine the exact anatomical location and the spatial extent of neuronal activity changes throughout the complete visual cortex as well as subcortical retinal targets, by measuring changes in the expression of the IEG *zif268*. A mouse-specific synthetic oligonucleotide probe (Eurogentec, Seraing, Belgium) for *zif268* was used as before with sequence 5′- CCGTTGCTCAGCAGCATCATCTCCTCCAGTTTG GGGTAGTTGTCC-3′.

As a first control, sets of tissue sections were hybridized with sense oligonucleotides in an identical manner to the antisense oligonucleotide probes. A competition experiment included the pre-hybridization of sets of tissue sections with a 50-fold excess of relevant or irrelevant unlabelled probe for 1 h prior to hybridization with labelled antisense probe. Some sections were incubated with RNase-containing buffer (0.005% RNase; Sigma-Aldrich; in 0.1 M phosphate buffer pH 7.4) for 1 h at 37 °C prior to hybridization with labelled probe. All control experiments, except the irrelevant probe test, abolished the signal as generated by normal antisense probe hybridization (Arckens *et al.*, 1995; Van Brussel *et al.*, 2009).

Each probe was 3′-end labelled with ^{33}P-dATP using terminal deoxynucleotidyl transferase (Invitrogen, Paisley, UK). Unincorporated nucleotides were separated from the labelled probe with mini-Quick Spin™ Oligo Columns (Roche Diagnostics, Brussels, Belgium). Series of cryostat sections for *zif268* were fixed, dehydrated and delipidated. The radioactively labelled probe was added to a hybridization cocktail [50% (vol/vol) formamide, 4× standard saline sodium citrate buffer, 1 × Denhardt's solution, 10% (wt/vol) dextran sulphate, 100 μg/mL herring sperm DNA, 250 μg/mL tRNA, 60 mM dithiothreitol, 1% (wt/vol) *N*-lauroyl sarcosine, 20 mM $NaHPO_4$, pH 7.4] and applied to the cryostat sections (10^6 c.p.m. per section) for an overnight incubation at 37 °C in a humid chamber. The following day, sections were rinsed in 1 × standard saline sodium citrate buffer at 42 °C, dehydrated, air-dried and exposed to an autoradiographic film (Biomax MR, Kodak). Films for *zif268* were developed in Kodak D19 developing solution after 6 days. Fixation was performed in Rapid fixer (Ilford Hypam, Kodak).

Autoradiographic images from the coronal sections were scanned at 1200 d.p.i. (CanoScan LIDE 600F, Canon) and all files were similarly adjusted for brightness and contrast in Adobe Photoshop CS5.

Histological verification of the position of LPZs in different visual areas

After *in situ* hybridization, all sections were counterstained with 1% cresyl violet (Fluka Chemical; Sigma-Aldrich) according to standard protocols. Cresyl violet provides sufficient information to delineate the different areas analysed, including primary visual cortex (V1), lateral extrastriate cortex (V2L), medial extrastriate cortex (V2M), rostromedial areas (RM), and agranular and granular retrosplenial cortex (RSA/RSG) (Fig. 2A) as described in detail previously (Van Der Gucht *et al.*, 2007; Van Brussel *et al.*, 2009, 2011; Nys *et al.*, 2014, 2015). All topographic denominations were adopted from these papers. Comparisons were made with the stereotaxic mouse brain atlas (Franklin & Paxinos, 2008).

Defining the extent of the LPZ along the anterior–posterior axis in V1/V2M and SC over time

The anterior and posterior borders of the LPZ in V1/V2M and the superior colliculus (SC) were determined on series of *in situ* hybridization sections of mice with different survival times (RL 2 days, 1 week, 3 weeks, 4 weeks and 8 weeks) by comparing these images with the atlas of the mouse brain (Franklin & Paxinos, 2008). Based on these Bregma levels, the mean extent of the LPZ along the anterior–posterior axis was calculated for all animals by multiplying the number of sections displaying the lesion by their thickness, taking the intersection interval into account.

Microscopy

Images of the stained retinae and coronal brain sections were obtained at 5 × (NA: 0.16) with a light microscope (Zeiss Axio Imager Z1) equipped with an AxioCam MRm camera (1388 × 1040 pixels) using the software program Axiovision Rel. 4.6 (Carl Zeiss-Benelux).

Quantitative analysis of in situ hybridization results

The optical density (OD) values (mean grey value per pixel) from the autoradiograms of three animals for each condition (RL 2 days, 1 week and 3 weeks, and CM) were quantified using a custom-made MATLAB script (MATLAB R2008b, The MathWorks Inc., Natick, MA, USA) as described earlier (Nys *et al.*, 2014). For each mouse, three 25-μm sections were selected around −3.52 mm relative to Bregma (Franklin & Paxinos, 2008). To demarcate the region of interest in the left hemisphere, we determined the top edge of the cortex, the border between the granular layer IV and infragranular layer V and the boundary where layer VI meets the white matter. These layer-related borders were computed by a contour-smoothing algorithm based on the Gaussian-weighted least squares fit (Birdal, 2011) from manually drawn lines on the autoradiogram. The different areal boundaries as derived from Nissl patterns were subsequently registered to the curvature of the top and bottom boundaries. Next, the delineated region of interest was divided equally into 30 segments creating two lattices of 30 quadrangles, corresponding to the upper (II–IV) and lower (V–VI) layers. To compensate for possible variation in brain size and morphology, we translated the lattice on each autoradiogram over the cortical curvature, fixing the border of a specific segment to an areal border (the border between segment 20/21 and 21/22, for the upper and lower layers respectively, is area border V1/V2M). For segments 3–28 created this way, the relative OD was calculated as the mean grey value of all pixels within this quadrangle normalized to the mean grey value of a square measured in the thalamus (a defined region with no *zif268* expression above background). This procedure was required to compare autoradiograms across experiments (Nys *et al.*, 2014). Relative *zif268* expression was expressed in percentages based on the following formula: [1−(cortical *zif268*/thalamic background)] × 100.

We compared *zif268* expression between different experimental and control groups for upper and lower layers of the visual cortex separately. Furthermore, relative expression patterns were assessed along the anatomically defined visual subdivisions.

Statistics

For each condition, the extent of the retinal lesion and LPZ as well as data for relative *zif268* expression in each segment separately and

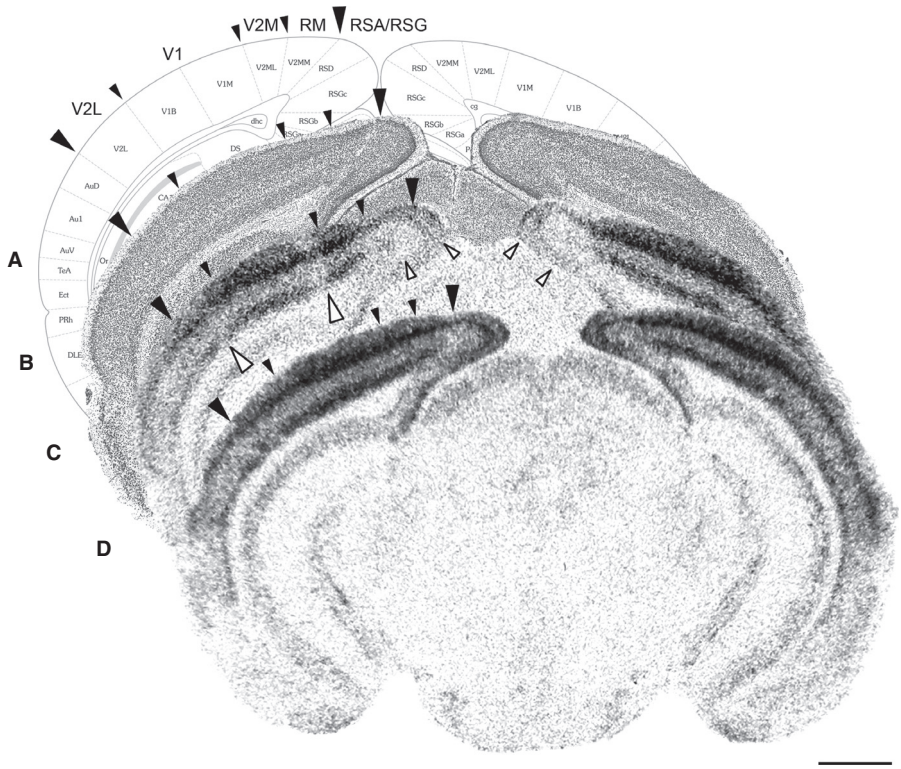

FIG. 2. Localization of the lesion projection zone in different visual cortical areas. (A) Bregma level −3.28 from the mouse brain atlas (Franklin & Paxinos, 2008). (B) Histological cresyl violet pattern delineating the visual cortex (large black arrowheads) and different areas within mouse visual cortex: the medial extrastriate cortex V2M, primary visual cortex V1, lateral extrastriate cortex V2L and rostromedial areas RM (small black arrowheads). (C) *zif268* expression pattern after visual stimulation of a retinal lesion mouse after 2 days of survival showing a lesion projection zone where contralaterally the monocular segment of V1 meets the V2M border and in scattered spots in contralateral V2L (large white arrowheads). Note also that expression decreases ipsilaterally and contralaterally in area RM and the agranular and granular retrosplenial cortex RSA/RSG (small white arrowheads). (D) *zif268* expression pattern of a visually stimulated control mouse. Scale bar: 1 mm.

for all segments in the LPZ are presented as mean ± standard error of the mean (SEM). As not all comparisons displayed a normal distribution of data points (Shapiro–Wilk test) within a group and with equal variance between groups and given the number of animals per group, non-parametric statistical tests were performed. The Kruskal–Wallis one-way analysis of variance on ranks test was used to analyse data of more than two conditions followed by a Tukey *post hoc* test for all pairwise multiple comparisons. When data coming from two conditions were analysed, a Mann–Whitney rank sum test for pairwise comparison of independent samples was applied. For all tests, the probability level (α-level was set to 0.05) of < 0.05 was accepted as statistically significant. Statistical analyses were performed using SigmaStat 3.1 (SYSTAT software).

Results

Localization of LPZs in the visual cortex

Lesions of 15° in visual angle were made dorso-nasally to the optic disc in the right retina of adult mice by focal laser photo-coagulation (Fig. 1A). To determine the number and position of possible LPZs in the visual cortex where neurons would cease to respond to visual stimulation, we performed *in situ* hybridization studies to detect localized expression changes for the activity reporter gene *zif268* (Fig. 2). This allowed us to distinguish a discrete zone of low IEG expression where the monocular segment of V1 meets the V2M border, and also less clearly delineated spots of low expression in V2L, contralateral to the lesioned eye in the first days following lesion. Areas RM and RSA/RSG displayed expression below normal levels ipsilateral as well as contralateral to the retinal lesion.

By performing *in situ* hybridization on series of sections and comparing these images with the atlas of the mouse brain (Franklin & Paxinos, 2008), the anterior and posterior margins of the LPZs in 2-day RL mice could be determined (Fig. 3A). The LPZ that encompassed the V1/V2M border was situated between Bregma levels −3.28 and −4.16, just anterior to the horizontal meridian representation across V1 according to the maps of Wang & Burkhalter (2007). The borders of the LPZ in RM extended even further, reaching maximally Bregma levels −3.16 at the anterior margin and −4.36 at the posterior border. The low expression levels in RSA/RSG were even noticeable along the full antero-posterior extent of the retrosplenial cortex. In V2L, however, delineating a clear LPZ was not possible as decreased expression was visible on only a few brain sections around Bregma level −3.52, not always adjacent to each other, giving it a distributed appearance in comparison with the V1/V2M LPZ.

Quantitative analysis of the *zif268* expression patterns in visual areas V1, V2M and V2L of 2-day RL mice vs. control mice confirmed the discrete LPZ in monocular V1 and encompassing the border with V2M (Fig. 4: Mann–Whitney rank sum test for pairwise comparison of independent samples; Fig. 4A, upper layers $T = 924.000$, $P = 0.002$; Fig. 4B, lower layers $T = 729.000$, $P = 0.004$). The size of the LPZ in the upper layers (Fig. 4A) was larger (segments 15–23) than that in the lower layers (segments

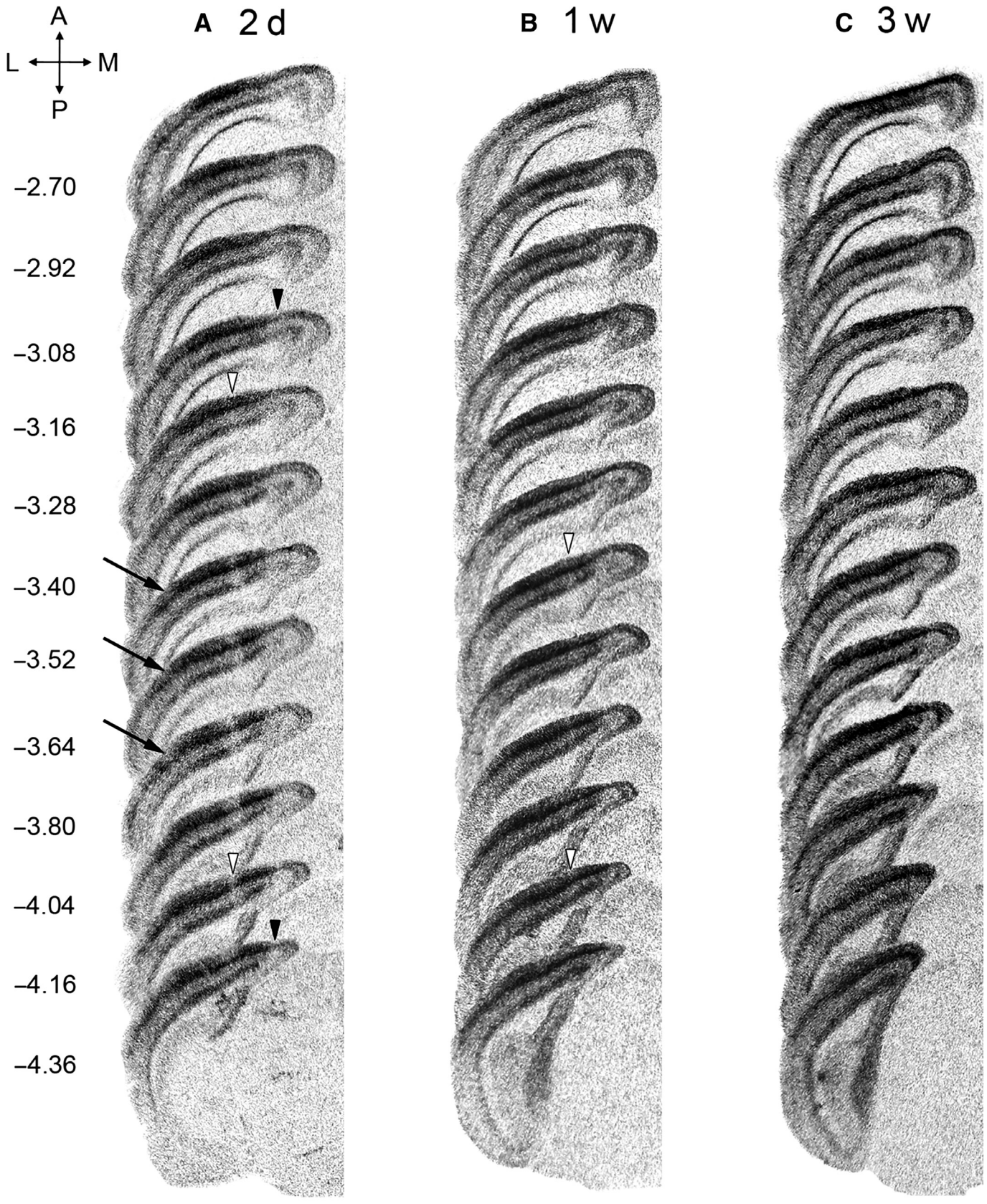

FIG. 3. Spatiotemporal pattern of the lesion projection zone in different cortical areas. Serial sections showing the *zif268* expression pattern in the contralateral visual cortex at 2 days (A), 1 week (B) and 3 weeks (C) following lesion. White and black arrowheads delineate the anterior and posterior border of the lesion projection zone (LPZ) in V1/V2M and RM, respectively. Black arrows point to the LPZ in V2L on discrete brain sections. Numbers to the left indicate corresponding Bregma levels. 2d, 2 days post-lesion; 1w, 1 week post-lesion; 3w, 3 weeks post-lesion; A, anterior; P, posterior; L, lateral; M, medial. Scale bar: 2 mm.

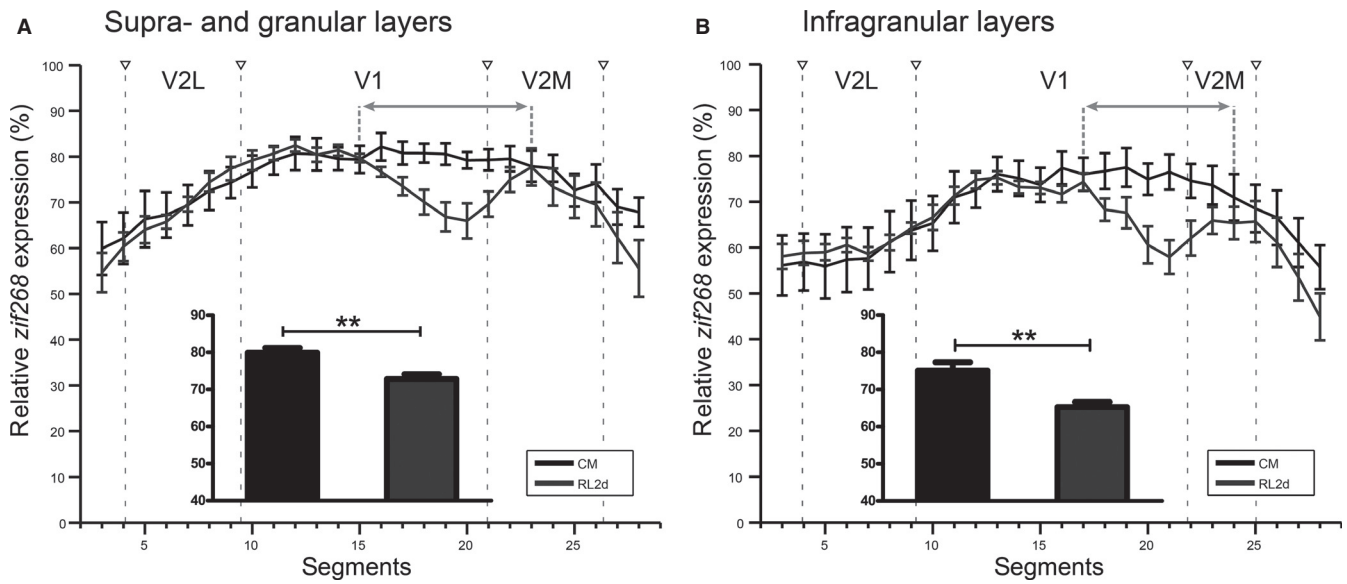

FIG. 4. A discrete region showing decreased *zif268* expression is present in the upper and lower layers where monocular V1 meets V2M 2 days following lesion. Line graphs illustrate the *zif268* expression in percentage relative to background levels around Bregma level −3.52 in the upper (II–IV) (A) and in the lower (V–VI) layers (B) along three predefined visual subdivisions, the lateral extrastriate cortex (V2L), primary visual cortex (V1) and medial extrastriate cortex (V2M) (white arrowheads), for control mice (CM, black) and retinal lesion mice with a survival time of 2 days (RL 2d, dark grey). Error bars represent the SEM of the mean relative *zif268* expression in each segment, calculated using a custom-made MATLAB script. The bar graphs with SEM show the mean relative *zif268* expression in percentage for the segments in the lesion projection zone (grey arrow). Statistics: Mann–Whitney rank sum test, $^{**}P < 0.01$.

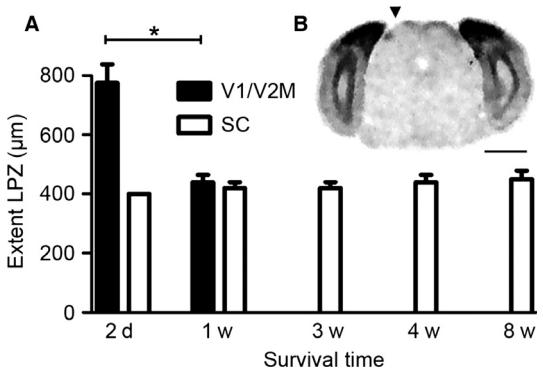

FIG. 5. Extent of the lesion projection zone along the anterior–posterior axis in V1/V2M and SC over time. (A) Mean extent of the LPZ (+ SEM) along the anterior–posterior axis in V1/V2M (black bars) and superior colliculus (SC) (white bars) over time, calculated for all animals per survival time. (B) Illustration of *zif268* expression pattern in a 2-day RL mouse. Black arrowhead indicates the lesion projection zone in the SC. Statistics: Mann–Whitney rank sum test, $^{*}P < 0.05$. V1, primary visual cortex; V2M, medial extrastriate cortex; 2d, 2 days post-lesion; 1w, 1 week post-lesion; 3w, 3 weeks post-lesion 4w; 4 weeks post-lesion; 8w, 8 weeks post-lesion. Scale bar: 2 mm.

17–24) (Fig. 4B), in accordance with its funnel-like appearance (Fig. 2B). In all layers, relative *zif268* expression gradually declined and increased when moving in and out of the LPZ, respectively (Fig. 4).

Recovery in the visual cortex

To investigate whether the cortical regions with low IEG expression were able to recover visually induced *zif268* expression over time, we performed *in situ* hybridization on sequential coronal brain sections of mice of different post-lesion survival times (Fig. 3). Figure 3B shows an apparent smaller LPZ in V1/V2M at 1 week when compared with 2 days post-lesion (Fig. 3A), with Bregma levels −3.52 and −4.16 demarcating the LPZ. By 3 weeks this LPZ was no longer discernible (Fig. 3C). The bar graph in Fig. 5A clearly shows the decrease of LPZ extent in V1/V2M caused by the retinal lesion over a period of 3 weeks (RL 2d – RL 1w: Mann–Whitney rank sum test for pairwise comparison of independent samples $T = 30.000$, $P = 0.016$). In V2L, RM and RSA/RSG, it is clear that *zif268* expression had already recovered within the first week following lesion (compare Fig. 3B and A).

The same reorganization trend in V1/V2M was visible after quantitative analysis (Fig. 6: Kruskal–Wallis one-way analysis of variance on ranks test with Tukey *post hoc* test; Fig. 6A, upper layers $H_3 = 35.628$, $P < 0.001$; $P < 0.05$ for CM – RL 2d & 1w; RL 3w – RL 2d & 1w; Fig. 6B, lower layers $H_3 = 42.085$, $P < 0.001$; $P < 0.05$ for CM – RL 2d; RL 3w – RL 2d & 1w). Moreover, this detailed comparison revealed that *zif268* expression exceeded control levels in the infragranular layers of the former LPZ 3 weeks after the lesion (Fig. 6B, lower layers: Kruskal–Wallis one way analysis of variance on ranks test followed by Tukey *post hoc* Test, $H_3 = 42.085$, $P < 0.001$; $P < 0.05$), suggesting a layer-specific response to the lesion.

Verification of the cortical nature of recovery

Next we determined whether the retina and an important direct retinal target structure in the mouse, the superior colliculus (SC), showed any sign of reorganization. Independent of survival time, the extent of the retinal lesion was on average 500 ± 47 μm, based on histology. This correlates well with the intended size, as 1° of visual angle corresponds to 31 μm in the mouse eye (Remtulla & Hallett, 1985). Figure 1B shows retinal cross-sections at

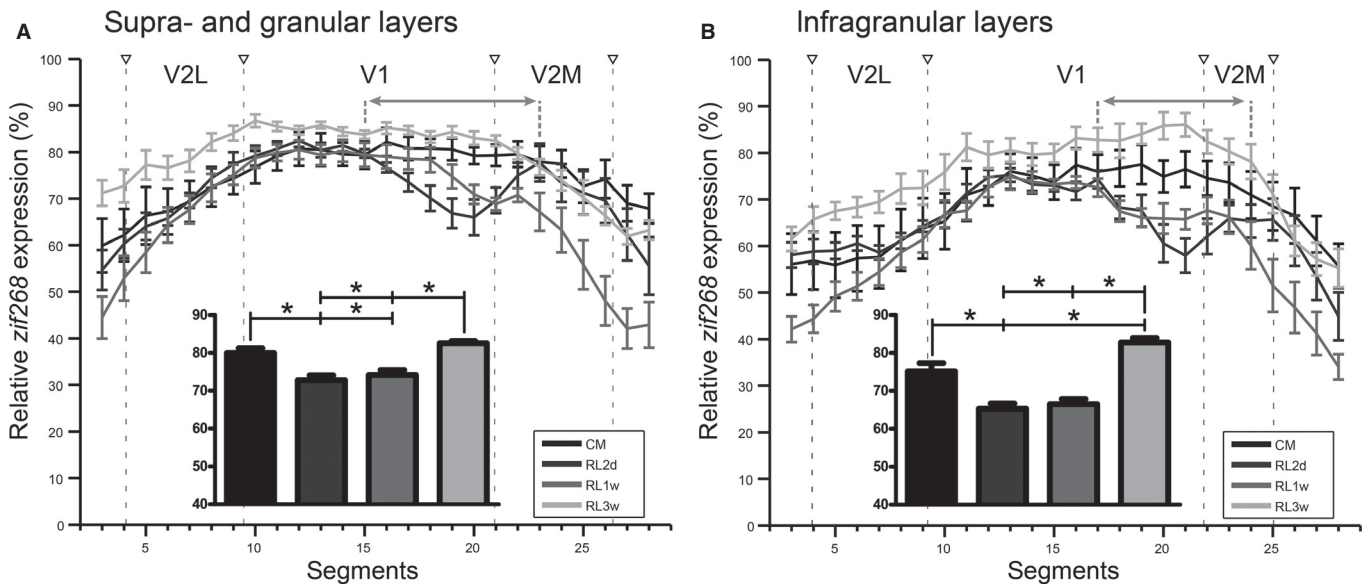

FIG. 6. Layer-specific reorganization in the visual cortex during the weeks following the retinal lesion. Line graphs illustrate the *zif268* expression in percentage relative to background levels around Bregma level −3.52 in the upper (II–IV) (A) and in the lower (V–VI) layers (B) along three predefined visual subdivisions, the lateral extrastriate cortex (V2L), primary visual cortex (V1) and medial extrastriate cortex (V2M) (white arrowheads), for control mice (CM, black) and retinal lesion mice with a survival time of 2 days (RL 2d, dark grey), 1 week (RL 1w, light gray) and 3 weeks (RL 3w, pale gray). Error bars represent the SEM of the mean relative *zif268* expression in each segment, calculated using a custom-made MATLAB script. The bar graphs with SEM show the mean relative *zif268* expression in percentage of the segments in the lesion projection zone (grey arrow). Statistics: Tukey *post hoc* test, $*P < 0.05$.

different positions within the lesion (panels 1–3). Comparison of the retinal morphology inside and outside the lesion zone demonstrated that the damage caused by the laser is not completely uniform. Beyond the lesioned area (Fig. 1B, panel 1), the different retinal layers were clearly visible including the ganglion cell layer (GCL), the inner plexiform layer (IPL), the inner nuclear layer (INL), the outer plexiform layer (OPL) the outer nuclear layer (ONL) and the layer of photoreceptor outer segments. The transition between normal and lesioned retina was rather gradual. At the border (Fig. 1B, panel 2), damage was mostly detected near the photoreceptor layer and GCL, whereas all retinal layers were affected near the centre (Fig. 1B, panel 3). Histology revealed anatomical features comparable to those found in cats with retinal laser lesions, which could indicate that the lesioned retinal tissue became scar tissue (Eysel *et al.*, 1981).

In the SC, *zif268* expression patterns allowed the localization of a clear and circumscribed LPZ in the upper optical layers. Its location in the lateral posterior part of the contralateral SC (Fig. 5B) is retinotopically correct, with an extent of approximately 400 μm between Bregma levels −4.04 and −4.48 in 2-day RL mice (Fig. 5A). To judge a possible recovery over time, we also examined the SC of RL mice 1–8 weeks after the lesion. The SC still showed a discrete zone of diminished *zif268* expression of comparable size and location to 2-day mice, thereby excluding any kind of recovery of subcortical visual experience-induced neuronal activity (Fig. 5A, Kruskal–Wallis one way analysis of variance on ranks, $H_4 = 3.149$, $P = 0.533$).

The *zif268* expression in the dorsal lateral geniculate nucleus (dLGN) of the thalamus was already extremely low in controls, making it impossible to judge any loss of signal due to the retinal lesion, as reported before in cat (Zhang *et al.*, 1994; Arckens *et al.*, 2000b), monkey (Soares *et al.*, 2005) and mouse (Takahata *et al.*, 2008). An earlier electrophysiological study in the cat described a spatially quite restricted functional recovery in the dLGN (Eysel, 1982).

Discussion

Employing *in situ* hybridization for *zif268* we demonstrated a decline in visually induced neuronal activity upon induction of an irreversible monocular retinal lesion in multiple regions throughout the cortex of the adult mouse. In ensuing weeks, full recovery of cortical *zif268* expression levels first occurred in higher order visual areas, but V1 also showed the capacity for a fast and complete intrinsic recovery.

zif268: a secondary indicator for neuronal activity changes in the visual system of mammals

Light stimulation after a period of darkness induces the rapid and transient expression of IEGs in the visual cortex of many mammalian species, including mouse (Worley *et al.*, 1991; Arckens *et al.*, 2000b; Correa-Lacarcel *et al.*, 2000; Mataga *et al.*, 2001; Van Der Gucht *et al.*, 2002). Glutamate receptor activation can increase cytosolic Ca^{2+} levels, influencing several signal transduction pathways that trigger the expression of, for example, the IEG *zif268* (Mataga *et al.*, 2001; Knapska & Kaczmarek, 2004; Soares *et al.*, 2005). As a regulatory transcription factor, Zif268 protein controls the expression of a diverse set of neuronal proteins (Knapska & Kaczmarek, 2004). Because synaptic activity regulates its expression, *zif268* acts as an excellent marker to map brain areas adapting their level of neuronal activity to changes in visual stimulation (Kaczmarek & Chaudhuri, 1997; Arckens *et al.*, 2000b, 2003; Massie *et al.*, 2003a,b; Qu *et al.*, 2003; Leysen *et al.*, 2004; Hu *et al.*, 2009; Van Brussel *et al.*, 2009, 2011; Woolley *et al.*, 2013; Nys *et al.*, 2014, 2015). Due to a relatively high basal expression level of *zif268* mRNA in adult visual cortex, both short- and long-term visual deprivation strategies can generate a measurable down-regulation of expression as well as its restoration to normal/higher levels by subsequent experience-induced stimulation (Kaczmarek & Chaudhuri, 1997). In monkey visual cortex, preferential expression

of Zif268 protein in excitatory neurons has been demonstrated (Chaudhuri *et al.*, 1995; Kaczmarek & Chaudhuri, 1997). Combined with the notion that *zif268* expression can be tightly regulated by pharmacologically manipulating excitatory transmission (Saffen *et al.*, 1988; Cole *et al.*, 1989; Worley *et al.*, 1991; Mataga *et al.*, 2001), we interpret the *in situ* hybridization experiments for *zif268* as a screening for brain regions showing alterations in synaptic activity of predominantly excitatory neurons over time in response to visual deprivation.

Position and size of LPZs in the visual cortex: indicators of retinotopy and cortical magnification factor

Within V1 the location of the LPZ is consistent with previously reported retinotopic maps, in which ganglion cells located in the upper nasal retina, and which receive information about the peripheral lower visual field, project to more anterior and medial parts of V1 (Dräger, 1975; Wagor *et al.*, 1980; Schuett *et al.*, 2002; Kalatsky & Stryker, 2003; Wang & Burkhalter, 2007; Bonin *et al.*, 2011; Marshel *et al.*, 2011; Garrett *et al.*, 2014). The position of this LPZ at the V1/V2M border also matches the position of the lower temporal visual field representation at the transition zone of V1 with the posteromedial area (Wang & Burkhalter, 2007; Garrett *et al.*, 2014).

Only recently, Garrett *et al.* (2014) reported the absence of a representation of the lower visual field in several mouse visual areas, which explains the lack of evidence for a clear LPZ in several higher order areas. The very small and distributed zones with reduced *zif268* expression which we located in extrastriate visual cortex lateral to V1 indeed confirm that several higher order visual areas in the mouse may not contain a full representation of the visual field. Consistent with this interpretation, and with their position around Bregma level −3.64, these small LPZs would be situated where the lateromedial (LM), laterointermediate (LI), and the anterolateral (AL) areas meet in the elevation maps of Garrett *et al.* (2014).

The size of the cortical LPZ was not previously specifically measured in mice after retinal lesions. Calculations using the cortical magnification factors obtained by Schuett *et al.* (2002) for V1 (mediolateral 14.5 ± 5.4 μm/°, anterior–posterior 24.8 ± 5.9 μm/°) predict a medio-lateral width of the LPZ in V1 in the range 225–300 μm ± 37% and an anterior–posterior extent of 372–440 μm ± 24%. These predictions fit the mediolateral range of the LPZ shown with *zif268* in V1 in Fig. 2B but underestimate the anterior–posterior size of the LPZ after 2 days as shown in Fig. 5A. However, the detailed mapping of 11 mouse visual areas and their cortical magnification factor using optical imaging (Garrett *et al.*, 2014) suggests differences in magnification factor across a given area. For V1, this demonstrates a larger magnification factor along the anterior–posterior axis of the brain exactly at the border between V1 and more medial visual cortex, and thus at the position of the elongated V1/V2M LPZ.

In binocular vision animals such as cats and monkeys, monocular retinal lesions have been described to have an impact on neuronal activity only in the monocular parts of the cortex situated in the contralateral hemisphere (Rosa *et al.*, 1995). Obviously, the fellow eye compensates for the visual deficit in largely binocular-driven visual cortex, an observation strengthened by investigations where the fellow eye has been removed to dissect the impact of monocular retinal lesions on visual cortex activation and plasticity (Kaas *et al.*, 1990). In our mice, a monocular retinal lesion did induce a clear zone with decreased *zif268* expression in ipsilateral and contralateral RM areas, the transition zone between the retrosplenial areas and area V2M, despite the binocular input to this area (Wagor *et al.*, 1980; Van Der Gucht *et al.*, 2007; Van Brussel *et al.*, 2009, 2011). Area RM is the medially located extrastriate cortical region that corresponds to V2MM in the atlas of the mouse brain (Franklin & Paxinos, 2008) and the mediomedial area (MM) in the maps of Wang & Burkhalter (2007). Although Wang & Burkhalter (2007) could only weakly label connections between V1 and this area, our results and previous studies in our lab suggest that this area responds very strongly to visual deprivation, just like areas RSA/RSG (Van Der Gucht *et al.*, 2007; Van Brussel *et al.*, 2009, 2011; Nys *et al.*, 2014). Optical imaging also revealed visual responsiveness in this cortical zone medial to V2M but no retinotopy (Garrett *et al.*, 2014), a finding that can explain our observations of a bilateral, more widespread rather than localized impact of the partial vision loss on *zif268* expression.

Rapid functional recovery in the visual cortex

The LPZ in V1/V2M regained visual *zif268* induction within 3 weeks following lesion. This result corresponds to the first period of rapid retinotopic and structural reorganization revealed by Keck *et al.* (2008) using intrinsic-signal imaging in mouse visual cortex after a unilateral retinal lesion of similar position but larger size. During the first month after the lesion, apical dendritic tufts of layer V pyramidal cells in the LPZ showed a 3.5-fold increase in spine turnover. The new spines probably form the structural basis for the rapid functional reorganization of the LPZ in contralateral monocular V1 (Keck *et al.*, 2008). Even when adult mice undergo monocular enucleation, contralateral V1 can still regain a normal *zif268* expression pattern, with the fellow-eye-driven reorganization component responsible for the expansion of the binocular cortex into monocular territory also occurring in the first 3 weeks following enucleation (Van Brussel *et al.*, 2011; Nys *et al.*, 2014, 2015).

The swiftness of recovery, and also the completeness, could be related to the large receptive fields of V1 cortical neurons in mice compared with monkeys (Niell & Stryker, 2008; Gao *et al.*, 2010; Van den Bergh *et al.*, 2010; Vreysen *et al.*, 2012), a hypothesis that could be tested via future in-depth analysis of the response to binocular retinal lesions of higher order visual areas in higher order binocular vision mammals. Shao *et al.* (2013) have already demonstrated that area MT in monkeys has a higher potential for reorganization after macular degeneration than V1, and higher order visual areas in rodents also exhibit much larger receptive fields than area V1 (Huang *et al.*, 2007; Van den Bergh *et al.*, 2010; Vermaercke *et al.*, 2014). The observation that the V1/V2M LPZ was the last to fully recover visual responsiveness may also be related to the cortical magnification factor being the largest along the anterior–posterior axis exactly at the border where V1 meets V2M (Garrett *et al.*, 2014), indicating that the largest cortical surface had to be reorganized.

Previous investigations dealing with *zif268* expression levels as an indicator of recovery of visually driven neuronal activity reported *zif268* levels exceeding normal values exactly in those parts of the visual cortex that undergo spatio-temporally matching binocular lesion-induced changes in excitability as measured by electrophysiology (Arckens *et al.*, 2000b; Giannikopoulos & Eysel, 2006; Hu *et al.*, 2009, 2011). Imbrosci *et al.* (2015) observed *zif268* levels above control in transhemispheric diaschysis, paralleled by a shift in the excitatory–inhibitory balance in favour of excitability as detected by *in vitro* patch-clamp recordings. In cats with binocular retinal lesions, the location and timing of abnormally high cortical IEG expression matched the LPZ border of intense receptive field remapping (Arckens *et al.*, 2000b). In the current mouse study, the

observation of such an increase in *zif268* levels above control at the LPZ site itself therefore fits the interpretation that this is the part of the mouse visual cortex where functional recovery exactly takes place, making it a plausible counterpart for the LPZ border in higher order mammals such as cat and monkey for future investigations about the cell-type-specific contribution to adult visual cortex plasticity.

A role for inhibition in lesion-induced adult cortex plasticity

Mechanistically, the retinal lesion may lower the threshold of predominant contralateral visually driven cells in the visual cortex, allowing formerly weak ipsilateral as well as top-down visually driven synapses to promote the reorganization. Indeed, previous studies have shown that acute reduction of inhibition reveals the presence of sub-threshold synaptic inputs to cortical neurons (Jacobs & Donoghue, 1991; Harauzov *et al.*, 2010; Keck *et al.*, 2011). So far the only evidence for a change in the mouse inhibitory circuit has come from V1 investigations. Within the first hours after the lesion, the inhibitory spine density decreases in the supragranular layers of V1 followed by that of the inhibitory boutons. The decrease is strongest in the centre but also occurs outside the LPZ, although with a gradual decline when moving further away from the lesion projection zone (Keck *et al.*, 2011). This pattern of inhibitory spine and bouton dynamics is consistent with our optical density measurements of the *zif268* signal, which revealed a gradual decrease from the border regions into the centre of the LPZ. Upon lesion induction, the resulting lowered overall inhibitory drive thus possibly triggers excitatory changes to accomplish the reorganization consistent with the detected increase in *zif268* expression levels 3 weeks after visual manipulation. The supragranular and infragranular layers in the V1/V2M LPZ displayed a differential time-dependent recovery profile upon deprivation, with an increase in expression reaching control levels or even higher levels, respectively. This layer-specific effect was also observed in area 17 of retinal lesion cats, by both electrophysiology and IEG detection (Waleszczyk *et al.*, 2003; Hu *et al.*, 2010), or upon monocular enucleation in mouse visual cortex (Van Brussel *et al.*, 2011; Nys *et al.*, 2014) and can be attributed to the layer-dependent distribution of glutamate receptors (Waleszczyk *et al.*, 2003; Hu *et al.*, 2010) that causes the layer-specific *zif268* expression. However, whereas infragranular layers recover faster and more extensively in mice, as suggested by the funnel-like shape of the *zif268* expression pattern in relation to the V1/V2M LPZ, the opposite holds in cats where supragranular layers were witnessed to recover deeper into the LPZ than infragranular layers (Arckens *et al.*, 2000b).

A permanent LPZ in the superior colliculus

The lateral posterior location of the LPZ in the SC is in accordance with previous mapping studies which show that the temporal part of the contralateral visual field projects posteriorly, and the inferior visual field laterally in the SC of the mouse (Dräger & Hubel, 1975, 1976). In contrast to the visual cortex, the SC showed no signs of recovery, not even after 8 weeks. In newborn rodents reorganization of retinocollicular projections can be induced by a retinal or optic tract lesion, or unilateral enucleation, resulting in an aberrant projection of ipsilateral retinal ganglion cell axons of the intact eye to the SC (Lund *et al.*, 1973; Lund & Lund, 1976; Godement *et al.*, 1980; Serfaty & Linden, 1991; Hanson & Reese, 1993; Serfaty *et al.*, 2005). In adult rodents, however, this reorganization of retinocollicular projections does not occur (Lund *et al.*, 1973; Lund & Lund, 1976), unless induced experimentally (Tropea *et al.*, 2003; Cancedda *et al.*, 2004; Landi *et al.*, 2007; Caleo *et al.*, 2009).

In conclusion, a discrete monocular retinal lesion immediately influences neuronal activity throughout all cortical layers of more than one area within adult mouse visual cortex. With time, the visual areas display the intrinsic capacity to reorganize and this persists well into adulthood, at a time when the capacity for ocular dominance plasticity has substantially decreased. The speed of the recovery mirrors cortical magnification factor, receptive field size and retinotopic organization. Interestingly, in mouse visual cortex the absence of a clear LPZ reflects an incomplete or partially condensed visual field representation for areas lateral to V1 and the absence of retinotopic organization in areas medial to V2M, as recently also witnessed using an optical imaging approach (Garrett *et al.*, 2014). The validation of this rodent model for deprivation-induced cortical plasticity may facilitate new investigations towards a better understanding of brain-region-, cell-type- and microcircuit-specific contributions to different forms of neuronal plasticity.

Conflict of interest

The authors declare that they have no conflict of interest.

Acknowledegements

This work was supported by grants of the Fund for Scientific Research – Flanders, Belgium (FWO), the Research Fund of the KU Leuven, Belgium (OT 09/022) and the German Research Foundation (DFG SFB 874, TP A2), a PhD fellowship of the Agency for Innovation through Science and Technology Flanders (IWT Vlaanderen, 101421) to K.S., an FRQS postdoctoral fellowship (FF6-14P/27498) and an FWO postdoctoral fellowship (12I7 316N/16144) to M.E.L., and an FWO Flanders PhD grant to A.C. and J.N. We thank Ria Vanlaer and Lieve Geenen for excellent technical assistance.

Abbreviations

CM, control mouse; dLGN, dorsal lateral geniculate nucleus; GCL, ganglion cell layer; IEG, immediate early gene; INL, inner nuclear layer; IPL, inner plexiform layer; LPZ, lesion projection zone; OD, optical density; ONL, outer nuclear layer; OPL, outer plexiform layer; RL, retinal lesion; RM, rostromedial areas; RSA/RSG, agranular and granular retrosplenial cortex; SC, superior colliculus; V1, primary visual cortex; V2L, lateral extrastriate cortex; V2M, medial extrastriate cortex.

References

Arckens, L., Zhang, F., Vanduffel, W., Mailleux, P., Vanderhaeghen, J.J., Orban, G.A. & Vandesande, F. (1995) Localization of the two protein kinase C beta-mRNA subtypes in cat visual system. *J. Chem. Neuroanat.*, **8**, 117–124.

Arckens, L., Schweigart, G., Qu, Y., Wouters, G., Pow, D.V., Vandesande, F., Eysel, U.T. & Orban, G.A. (2000a) Cooperative changes in GABA, glutamate and activity levels: the missing link in cortical plasticity. *Eur. J. Neurosci.*, **12**, 4222–4232.

Arckens, L., Van Der Gucht, E., Eysel, U.T., Orban, G.A. & Vandesande, F. (2000b) Investigation of cortical reorganization in area 17 and nine extrastriate visual areas through the detection of changes in immediate early gene expression as induced by retinal lesions. *J. Comp. Neurol.*, **425**, 531–544.

Arckens, L., Van Der Gucht, E., Van den Bergh, G., Massie, A., Leysen, I., Vandenbussche, E., Eysel, U.T., Huybrechts, R. & Vandesande, F. (2003) Differential display implicates cyclophilin A in adult cortical plasticity. *Eur. J. Neurosci.*, **18**, 61–75.

Birdal, T. (2011) Smoothing 2D contours using local regression lines. MATLAB Central File Exchange.Available at:http://www.mathworks.-com/matlabcentral/fileexchange/30793-smoothing-2d-contours-using-local-regression-lines.

Bonin, V., Histed, M.H., Yurgenson, S. & Reid, R.C. (2011) Local diversity and fine-scale organization of receptive fields in mouse visual cortex. *J. Neurosci.*, **31**, 18506–18521.

Buonomano, D.V. & Merzenich, M.M. (1998) Cortical plasticity: from synapses to maps. *Annu. Rev. Neurosci.*, **21**, 149–186.

Caleo, M., Tropea, D., Rossi, C., Gianfranceschi, L. & Maffei, L. (2009) Environmental enrichment promotes fiber sprouting after deafferentation of the superior colliculus in the adult rat brain. *Exp. Neurol.*, **216**, 515–519.

Cancedda, L., Putignano, E., Sale, A., Viegi, A., Berardi, N. & Maffei, L. (2004) Acceleration of visual system development by environmental enrichment. *J. Neurosci.*, **24**, 4840–4848.

Chaudhuri, A., Matsubara, J.A. & Cynader, M.S. (1995) Neuronal activity in primate visual cortex assessed by immunostaining for the transcription factor Zif268. *Vis. Neurosci.*, **12**, 35–50.

Chino, Y.M. (1995) Adult plasticity in the visual system. *Can. J. Physiol. Pharm.*, **73**, 1323–1338.

Chino, Y.M., Kaas, J.H., Smith, E.L. III, Langston, A.L. & Cheng, H. (1992) Rapid reorganization of cortical maps in adult cats following restricted deafferentation in retina. *Vision. Res.*, **32**, 789–796.

Chino, Y.M., Smith, E.L. III, Kaas, J.H., Sasaki, Y. & Cheng, H. (1995) Receptive-field properties of deafferentated visual cortical neurons after topographic map reorganization in adult cats. *J. Neurosci.*, **15**, 2417–2433.

Cole, A.J., Saffen, D.W., Baraban, J.M. & Worley, P.F. (1989) Rapid increase of an immediate early gene messenger RNA in hippocampal neurons by synaptic NMDA receptor activation. *Nature*, **340**, 474–476.

Correa-Lacarcel, J., Pujante, M.J., Terol, F.F., Almenar-Garcia, V., Puchades-Orts, A., Ballesta, J.J., Lloret, J., Robles, J.A. & Sanchez-del-Campo, F. (2000) Stimulus frequency affects c-fos expression in the rat visual system. *J. Chem. Neuroanat.*, **18**, 135–146.

Das, A. & Gilbert, C.D. (1995a) Long-range horizontal connections and their role in cortical reorganization revealed by optical recording of cat primary visual cortex. *Nature*, **375**, 780–784.

Das, A. & Gilbert, C.D. (1995b) Receptive field expansion in adult visual cortex is linked to dynamic changes in strength of cortical connections. *J. Neurophysiol.*, **74**, 779–792.

Dräger, U.C. (1975) Receptive fields of single cells and topography in mouse visual cortex. *J. Comp. Neurol.*, **160**, 269–290.

Dräger, U.C. & Hubel, D.H. (1975) Responses to visual stimulation and relationship between visual, auditory, and somatosensory inputs in mouse superior colliculus. *J. Neurophysiol.*, **38**, 690–713.

Dräger, U.C. & Hubel, D.H. (1976) Topography of visual and somatosensory projections to mouse superior colliculus. *J. Neurophysiol.*, **39**, 91–101.

Dreher, B., Burke, W. & Calford, M.B. (2001) Cortical plasticity revealed by circumscribed retinal lesions or artificial scotomas. *Prog. Brain Res.*, **134**, 217–246.

Eysel, U.T. (1982) Functional reconnections without new axonal growth in a partially denervated visual relay nucleus. *Nature*, **299**, 442–444.

Eysel, U.T., Gonzalez-Aguilar, F. & Mayer, U. (1981) Time-dependent decrease in the extent of visual deafferentation in the lateral geniculate nucleus of adult cats with small retinal lesions. *Exp. Brain Res.*, **41**, 256–263.

Franklin, G. & Paxinos, K. (2008) *The Mouse Brain in Stereotaxic Coordinates*. Elsevier, Amsterdam.

Gao, E., DeAngelis, G.C. & Burkhalter, A. (2010) Parallel input channels to mouse primary visual cortex. *J. Neurosci.*, **30**, 5912–5926.

Garrett, M.E., Nauhaus, I., Marshel, J.H. & Callaway, E.M. (2014) Topography and areal organization of mouse visual cortex. *J. Neurosci.*, **34**, 12587–12600.

Giannikopoulos, D.V. & Eysel, U.T. (2006) Dynamics and specificity of cortical map reorganization after retinal lesions. *Proc. Natl Acad. Sci. USA*, **103**, 10805–10810.

Gilbert, C.D. & Wiesel, T.N. (1992) Receptive field dynamics in adult primary visual cortex. *Nature*, **356**, 150–152.

Godement, P., Saillour, P. & Imbert, M. (1980) The ipsilateral optic pathway to the dorsal lateral geniculate nucleus and superior colliculus in mice with prenatal or postnatal loss of one eye. *J. Comp. Neurol.*, **190**, 611–626.

Hanson, E.S. & Reese, B.E. (1993) Rapid plastic response following early retinal lesions in rats. *Brain Res. Dev. Brain Res.*, **73**, 293–298.

Harauzov, A., Spolidoro, M., DiCristo, G., De, P.R., Cancedda, L., Pizzorusso, T., Viegi, A., Berardi, N. & Maffei, L. (2010) Reducing intracortical inhibition in the adult visual cortex promotes ocular dominance plasticity. *J. Neurosci.*, **30**, 361–371.

Heinen, S.J. & Skavenski, A.A. (1991) Recovery of visual responses in foveal V1 neurons following bilateral foveal lesions in adult monkey. *Exp. Brain Res.*, **83**, 670–674.

Hofer, S.B., Mrsic-Flogel, T.D., Bonhoeffer, T. & Hubener, M. (2006a) Lifelong learning: ocular dominance plasticity in mouse visual cortex. *Curr. Opin. Neurobiol.*, **16**, 451–459.

Hofer, S.B., Mrsic-Flogel, T.D., Bonhoeffer, T. & Hubener, M. (2006b) Prior experience enhances plasticity in adult visual cortex. *Nat. Neurosci.*, **9**, 127–132.

Hu, T.T., Laeremans, A., Eysel, U.T., Cnops, L. & Arckens, L. (2009) Analysis of c-fos and zif268 expression reveals time-dependent changes in activity inside and outside the lesion projection zone in adult cat area 17 after retinal lesions. *Cereb. Cortex*, **19**, 2982–2992.

Hu, T.T., Van Der Gucht, E., Eysel, U.T. & Arckens, L. (2010) Retinal lesions induce layer-specific Fos expression changes in cat area 17. *Exp. Brain Res.*, **205**, 139–144.

Hu, T.T., Van den Bergh, G., Thorrez, L., Heylen, K., Eysel, U.T. & Arckens, L. (2011) Recovery from retinal lesions: molecular plasticity mechanisms in visual cortex far beyond the deprived zone. *Cereb. Cortex*, **21**, 2883–2892.

Huang, J.Y., Wang, C. & Dreher, B. (2007) The effects of reversible inactivation of postero-temporal visual cortex on neuronal activities in cat's area 17. *Brain Res.*, **1138**, 111–128.

Huberman, A.D. & Niell, C.M. (2011) What can mice tell us about how vision works? *Trends Neurosci.*, **34**, 464–473.

Imbrosci, B., Ytebrouck, E., Arckens, L. & Mittmann, T. (2015) Neuronal mechanisms underlying transhemispheric diaschisis following focal cortical injuries. *Brain Struct. Funct.*, **220**, 1649–1664.

Jacobs, K.M. & Donoghue, J.P. (1991) Reshaping the cortical motor map by unmasking latent intracortical connections. *Science*, **251**, 944–947.

Kaas, J.H. (1991) Plasticity of sensory and motor maps in adult mammals. *Annu. Rev. Neurosci.*, **14**, 137–167.

Kaas, J.H., Krubitzer, L.A., Chino, Y.M., Langston, A.L., Polley, E.H. & Blair, N. (1990) Reorganization of retinotopic cortical maps in adult mammals after lesions of the retina. *Science*, **248**, 229–231.

Kaczmarek, L. & Chaudhuri, A. (1997) Sensory regulation of immediate-early gene expression in mammalian visual cortex: implications for functional mapping and neural plasticity. *Brain Res. Brain Res. Rev.*, **23**, 237–256.

Kalatsky, V.A. & Stryker, M.P. (2003) New paradigm for optical imaging: temporally encoded maps of intrinsic signal. *Neuron*, **38**, 529–545.

Keck, T., Mrsic-Flogel, T.D., Vaz, A.M., Eysel, U.T., Bonhoeffer, T. & Hubener, M. (2008) Massive restructuring of neuronal circuits during functional reorganization of adult visual cortex. *Nat. Neurosci.*, **11**, 1162–1167.

Keck, T., Scheuss, V., Jacobsen, R.I., Wierenga, C.J., Eysel, U.T., Bonhoeffer, T. & Hubener, M. (2011) Loss of sensory input causes rapid structural changes of inhibitory neurons in adult mouse visual cortex. *Neuron*, **71**, 869–882.

Knapska, E. & Kaczmarek, L. (2004) A gene for neuronal plasticity in the mammalian brain: Zif268/Egr-1/NGFI-A/Krox-24/TIS8/ZENK? *Prog. Neurobiol.*, **74**, 183–211.

Landi, S., Sale, A., Berardi, N., Viegi, A., Maffei, L. & Cenni, M.C. (2007) Retinal functional development is sensitive to environmental enrichment: a role for BDNF. *FASEB J.*, **21**, 130–139.

Leysen, I., Van Der Gucht, E., Eysel, U.T., Huybrechts, R., Vandesande, F. & Arckens, L. (2004) Time-dependent changes in the expression of the MEF2 transcription factor family during topographic map reorganization in mammalian visual cortex. *Eur. J. Neurosci.*, **20**, 769–780.

Lund, R.D. & Lund, J.S. (1976) Plasticity in the developing visual system: the effects of retinal lesions made in young rats. *J. Comp. Neurol.*, **169**, 133–154.

Lund, R.D., Cunningham, T.J. & Lund, J.S. (1973) Modified optic projections after unilateral eye removal in young rats. *Brain Behav. Evolut.*, **8**, 51–72.

Marik, S.A., Yamahachi, H., Meyer zum Alten Borgloh, S. & Gilbert, C.D. (2014) Large-scale axonal reorganization of inhibitory neurons following retinal lesions. *J. Neurosci.*, **34**, 1625–1632.

Marshel, J.H., Garrett, M.E., Nauhaus, I. & Callaway, E.M. (2011) Functional specialization of seven mouse visual cortical areas. *Neuron*, **72**, 1040–1054.

Massie, A., Cnops, L., Jacobs, S., Van Damme, K., Vandenbussche, E., Eysel, U.T., Vandesande, F. & Arckens, L. (2003a) Glutamate levels and transport in cat (*Felis catus*) area 17 during cortical reorganization

following binocular retinal lesions. *J. Neurochem.*, **84**, 1387–1397.

Massie, A., Cnops, L., Smolders, I., Van Damme, K., Vandenbussche, E., Vandesande, F., Eysel, U.T. & Arckens, L. (2003b) Extracellular GABA concentrations in area 17 of cat visual cortex during topographic map reorganization following binocular central retinal lesioning. *Brain Res.*, **976**, 100–108.

Mataga, N., Fujishima, S., Condie, B.G. & Hensch, T.K. (2001) Experience-dependent plasticity of mouse visual cortex in the absence of the neuronal activity-dependent marker egr1/zif268. *J. Neurosci.*, **21**, 9724–9732.

Merzenich, M.M., Kaas, J.H., Wall, J., Nelson, R.J., Sur, M. & Felleman, D. (1983) Topographic reorganization of somatosensory cortical areas 3b and 1 in adult monkeys following restricted deafferentation. *Neuroscience*, **8**, 33–55.

Niell, C.M. & Stryker, M.P. (2008) Highly selective receptive fields in mouse visual cortex. *J. Neurosci.*, **28**, 7520–7536.

Nys, J., Aerts, J., Ytebrouck, E., Vreysen, S., Laeremans, A. & Arckens, L. (2014) The cross-modal aspect of mouse visual cortex plasticity induced by monocular enucleation is age dependent. *J. Comp. Neurol.*, **522**, 950–970.

Nys, J., Smolders, K., Laramée, M.E., Hofman, I., Hu, T.T. & Arckens, L. (2015) Regional specificity of GABAergic regulation of cross-modal plasticity in mouse visual cortex after unilateral enucleation. *J. Neurosci.*, **35**, 11174–11189.

Pham, T.A., Graham, S.J., Suzuki, S., Barco, A., Kandel, E.R., Gordon, B. & Lickey, M.E. (2004) A semi-persistent adult ocular dominance plasticity in visual cortex is stabilized by activated CREB. *Learn Memory*, **11**, 738–747.

Qu, Y., Massie, A., Van Der Gucht, E., Cnops, L., Vandenbussche, E., Eysel, U.T., Vandesande, F. & Arckens, L. (2003) Retinal lesions affect extracellular glutamate levels in sensory-deprived and remote non-deprived regions of cat area 17 as revealed by in vivo microdialysis. *Brain Res.*, **962**, 199–206.

Remtulla, S. & Hallett, P.E. (1985) A schematic eye for the mouse, and comparisons with the rat. *Vision. Res.*, **25**, 21–31.

Rosa, M.G.P., Schmid, L.M. & Calford, M.B. (1995) Responsiveness of cat area 17 after monocular inactivation: limitation of topographic plasticity in adult cortex. *J. Physiol.*, **482**, 589–608.

Saffen, D.W., Cole, A.J., Worley, P.F., Christy, B.A., Ryder, K. & Baraban, J.M. (1988) Convulsant-induced increase in transcription factor messenger RNAs in rat brain. *Proc. Natl Acad. Sci. USA*, **85**, 7795–7799.

Sawtell, N.B., Frenkel, M.Y., Philpot, B.D., Nakazawa, K., Tonegawa, S. & Bear, M.F. (2003) NMDA receptor-dependent ocular dominance plasticity in adult visual cortex. *Neuron*, **38**, 977–985.

Schuett, S., Bonhoeffer, T. & Hubener, M. (2002) Mapping retinotopic structure in mouse visual cortex with optical imaging. *J. Neurosci.*, **22**, 6549–6559.

Serfaty, C.A. & Linden, R. (1991) Evidence that the relative densities of afferents from both eyes control laminar distribution and binocular segregation of retinotectal projections in rats. *Brain Res. Dev. Brain Res.*, **60**, 9–17.

Serfaty, C.A., Campello-Costa, P. & Linden, R. (2005) Rapid and long-term plasticity in the neonatal and adult retinotectal pathways following a retinal lesion. *Brain Res. Bull.*, **66**, 128–134.

Shao, Y., Keliris, G.A., Papanikolaou, A., Fischer, M.D., Zobor, D., Jagle, H., Logothetis, N.K. & Smirnakis, S.M. (2013) Visual cortex organisation in a macaque monkey with macular degeneration. *Eur. J. Neurosci.*, **38**, 3456–3464.

Soares, J.G., Pereira, A.C., Botelho, E.P., Pereira, S.S., Fiorani, M. & Gattass, R. (2005) Differential expression of Zif268 and c-Fos in the primary visual cortex and lateral geniculate nucleus of normal *Cebus* monkeys and after monocular lesions. *J. Comp. Neurol.*, **482**, 166–175.

Tagawa, Y., Kanold, P.O., Majdan, M. & Shatz, C.J. (2005) Multiple periods of functional ocular dominance plasticity in mouse visual cortex. *Nat. Neurosci.*, **8**, 380–388.

Takahata, T., Hashikawa, T., Higo, N., Tochitani, S. & Yamamori, T. (2008) Difference in sensory dependence of occ1/Follistatin-related protein expression between macaques and mice. *J. Chem. Neuroanat.*, **35**, 146–157.

Tropea, D., Caleo, M. & Maffei, L. (2003) Synergistic effects of brain-derived neurotrophic factor and chondroitinase ABC on retinal fiber sprouting after denervation of the superior colliculus in adult rats. *J. Neurosci.*, **23**, 7034–7044.

Van Brussel, L., Gerits, A. & Arckens, L. (2009) Identification and localization of functional subdivisions in the visual cortex of the adult mouse. *J. Comp. Neurol.*, **514**, 107–116.

Van Brussel, L., Gerits, A. & Arckens, L. (2011) Evidence for cross-modal plasticity in adult mouse visual cortex following monocular enucleation. *Cereb. Cortex*, **21**, 2133–2146.

Van den Bergh, G., Zhang, B., Arckens, L. & Chino, Y.M. (2010) Receptive-field properties of V1 and V2 neurons in mice and macaque monkeys. *J. Comp. Neurol.*, **518**, 2051–2070.

Van Der Gucht, E., Clerens, S., Cromphout, K., Vandesande, F. & Arckens, L. (2002) Differential expression of c-fos in subtypes of GABAergic cells following sensory stimulation in the cat primary visual cortex. *Eur. J. Neurosci.*, **16**, 1620–1626.

Van Der Gucht, E., Hof, P.R., Van Brussel, L., Burnat, K. & Arckens, L. (2007) Neurofilament protein and neuronal activity markers define regional architectonic parcellation in the mouse visual cortex. *Cereb. Cortex*, **17**, 2805–2819.

Vermaercke, B., Gerich, F.J., Ytebrouck, E., Arckens, L., Op de Beeck, H.P. & Van den Bergh, G. (2014) Functional specialization in rat occipital and temporal visual cortex. *J. Neurophysiol.*, **112**, 1963–1983.

Vreysen, S., Zhang, B., Chino, Y.M., Arckens, L. & Van den Bergh, G. (2012) Dynamics of spatial frequency tuning in mouse visual cortex. *J. Neurophysiol.*, **107**, 2937–2949.

Wagor, E., Mangini, N.J. & Pearlman, A.L. (1980) Retinotopic organization of striate and extrastriate visual cortex in the mouse. *J. Comp. Neurol.*, **193**, 187–202.

Waleszczyk, W.J., Wang, C., Young, J.M., Burke, W., Calford, M.B. & Dreher, B. (2003) Laminar differences in plasticity in area 17 following retinal lesions in kittens or adult cats. *Eur. J. Neurosci.*, **17**, 2351–2368.

Wandell, B.A. & Smirnakis, S.M. (2009) Plasticity and stability of visual field maps in adult primary visual cortex. *Nat. Rev. Neurosci.*, **10**, 873–884.

Wang, Q. & Burkhalter, A. (2007) Area map of mouse visual cortex. *J. Comp. Neurol.*, **502**, 339–357.

Wiesel, T.N. & Hubel, D.H. (1963) Single-cell responses in striate cortex of kittens deprived of vision in one eye. *J. Neurophysiol.*, **26**, 1003–1017.

Woolley, D.G., Laeremans, A., Gantois, I., Mantini, D., Vermaercke, B., Op de Beeck, H.P., Swinnen, S.P., Wenderoth, N., Arckens, L. & D'Hooge, R. (2013) Homologous involvement of striatum and prefrontal cortex in rodent and human water maze learning. *Proc. Natl Acad. Sci. USA*, **110**, 3131–3136.

Worley, P.F., Christy, B.A., Nakabeppu, Y., Bhat, R.V., Cole, A.J. & Baraban, J.M. (1991) Constitutive expression of *zif268* in neocortex is regulated by synaptic activity. *Proc. Natl Acad. Sci. USA*, **88**, 5106–5110.

Yamahachi, H., Marik, S.A., McManus, J.N., Denk, W. & Gilbert, C.D. (2009) Rapid axonal sprouting and pruning accompany functional reorganization in primary visual cortex. *Neuron*, **64**, 719–729.

Young, J.M., Waleszczyk, W.J., Burke, W., Calford, M.B. & Dreher, B. (2002) Topographic reorganization in area 18 of adult cats following circumscribed monocular retinal lesions in adolescence. *J. Physiol.*, **541**, 601–612.

Zangenehpour, S. & Chaudhuri, A. (2002) Differential induction and decay curves of c-fos and zif268 revealed through dual activity maps. *Brain Res. Mol. Brain Res.*, **109**, 221–225.

Zhang, F., Halleux, P., Arckens, L., Vanduffel, W., Van Brussel, L., Mailleux, P., Vandesande, F., Orban, G.A. & Vanderhaeghen, J.J. (1994) Distribution of immediate early gene zif-268, c-fos, c-jun and jun-D mRNAs in the adult cat with special references to brain region related to vision. *Neurosci. Lett.*, **176**, 137–141.